Journal of Biophotonics

JOURNAL OF BIOPHOTONICS

RESEARCH ARTICLE OPEN ACCESS

Theranostic-Guided UV-A Light Corneal Wavefront Photo-Reshaping for Presbyopia Correction: A Preclinical Study

Marco Lombardo[1,2] | Giuseppe Massimo Bernava[3] | Sebastiano Serrao[1,2] | Giuseppe Lombardo[1,3]

[1]Studio Italiano di Oftalmologia, Rome, Italy | [2]Vision Engineering Italy srl, Rome, Italy | [3]CNR-IPCF, Istituto per i Processi Chimico-Fisici, Messina, Italy

Correspondence: Marco Lombardo (mlombardo@visioeng.it) | Giuseppe Lombardo (giuseppe.lombardo@cnr.it)

Received: 18 October 2024 | **Revised:** 14 November 2024 | **Accepted:** 18 November 2024

Funding: This work was partially funded by PR LAZIO FESR 2021/2027 Prog. no. A0613.2023.077528, CUP F89J23001100007 granted by Lazio Innova Spa.

Keywords: corneal iontophoresis | patterned drug delivery | presbyopia | riboflavin | theranostics

ABSTRACT

This study investigated the effect of a theranostic-guided UV-A light corneal photo-reshaping technique on corneal elevation and wavefront aberration (WA) in human donor eyes. A specialized platform, combining UV-A light with corneal iontophoresis for controlled, patterned, riboflavin delivery, was used for both distribution assessment and concentration-driven photopolymerization of corneal proteins. In all cases, a consistent riboflavin concentration gradient, with lower levels in the central prepupillary zone, was recorded. Corneal topography and WA measurements showed significant corneal steepening and smooth wavefront shaping, respectively, with a delay in the central 2.0 mm of the WA and advancement in the surrounding zone, as well as a 50% reduction in corneal spherical aberration over a 5.0 mm pupil size. Notably, the corneal optical quality, measured via modulation transfer function (MTF), remained stable. This incision-free approach demonstrated the potential to extend focal range without compromising distance vision, presenting a new solution for presbyopia correction.

1 | Introduction

Presbyopia is one of the most common causes of vision impairment, affecting nearly 2 billion people worldwide over the age of 40 [1]. Presbyopia is the loss or insufficiency of the accommodative ability of the eye. It is an irreversible, physiologic aging process that ultimately affects all humans. Estimated disability-adjusted life years and productivity loss studies indicated that uncorrected refractive error has a potentially greater impact on the global economy than all other preventable causes of moderate to severe vision impairment and blindness. The economic burden from uncorrected presbyopia has been associated with a potential productivity loss of US $11 billion per year [2].

In the last two decades, several surgical methodologies to correct presbyopia or to restore the accommodation have been developed to eliminate the dependence on reading glasses. These procedures are applied on the cornea, the crystalline lens, or the sclera. Effective correction of near vision in presbyopic patients should ensure the maintenance of distant vision acuity while promoting improved vision for near tasks.

Presbyopia correction can be achieved with excimer and/or femtosecond laser ablation on the cornea, using various software algorithms, such as PresbyLASIK, Supracor, Intracor, presbyMAX, and so forth, unilaterally as a monovision procedure or bilaterally [3–5]. The corneal laser approaches however reported a loss of two

Abbreviations: Abb1, abbreviation 1; CXL, corneal cross-linking.

Marco Lombardo and Giuseppe Lombardo should be considered joint first author.

lines of distance visual acuity in a high number of patients [6]. Another approach is the insertion of synthetic, or more recently, biological intrastromal inlays into the cornea through a femtosecond laser-assisted surgical procedure [7, 8]. Different designs of presbyopic corneal inlays have been proposed, including small aperture inlays that increase the depth-of-focus using the pin-hole effect, space-occupying inlays that create a hyperprolate cornea, and refractive annular addition lenticules that work as bifocal optical inlays [9]. However, long-term outcomes for synthetic prostheses revealed low levels of patient satisfaction, biocompatibility concerns, high explantation rates, and instances of spontaneous corneal extrusion [7, 10–12]. Conductive keratoplasty gained brief popularity as an in-office-based procedure but it proved to have limited efficacy due to its high regression rate [9, 13]. Lens extraction, involving the implantation of multifocal, monofocal (monovision), or accommodative intraocular lenses (IOLs), is another method for correcting presbyopia, however, it is primarily limited to patients with cataracts [14].

The number of different surgical techniques and the variety of approaches have arisen from the unsuccessful or partial effectiveness of methods developed to restore true accommodation or at least to improve near visual acuity. For these reasons, pharmacological treatment of presbyopia using topical parasympathetic drugs or other agents, to contract the ciliary and pupil muscle and potentially restore the accommodation, has been recently proposed for improvement of uncorrected near visual acuity, although there are a few reports on adverse effects caused by prolonged use of these agents, including, for example, headache and reduced distance vision [11, 15].

Current corneal approaches to presbyopia surgical correction rely on empirical methods to enhance "pseudo-accommodation" by changing corneal thickness to extend depth-of-focus and exploit a technique that dates back to the mid of 1900 [16]. This is obtained, by removing own tissue (e.g., corneal ablation or photo-disruption) or adding (e.g., corneal inlays) allograft tissue or biomaterial, to modify the optical length of light entering the eye. Emerging solutions using UV-A light and riboflavin, designed to reorganize the corneal tissue microstructure, could enhance the optical properties of the cornea to compensate for the loss of lens accommodation without the need for tissue removal or incisions. Preclinical and clinical studies have shown that under targeted theranostic-guided UV-A light photo-activation, the concentration distribution of riboflavin in the cornea plays a crucial role in generating new covalent chemical bonds between stromal proteins, as previously theorized by researchers [17–19]. Theranostics technology has proven to provide a precise and reliable method for significantly improving corneal tissue strength and anterior corneal flattening in patients with keratoconus treated by corneal cross-linking (CXL) using riboflavin and UV-A light [20–22]. A previous laboratory study demonstrated that theranostic UV-A-induced photoactivation of a patterned riboflavin concentration in the cornea, delivered through a controlled iontophoresis system with a central aperture wider than the surrounding apertures, produced a predictable and reproducible corneal shape change, effectively correcting myopic defocus [23].

This study aimed to evaluate the feasibility of theranostic-guided UV-A light corneal photo-reshaping for presbyopia correction. The approach combines patterned riboflavin delivery with concentration-driven photopolymerization of stromal proteins. The hypothesis of the study was that spatially patterned delivery of riboflavin, with higher and consistent concentration levels in the peripupillary area compared to the prepupillary area, combined with theranostic-guided UV-A light irradiation, would reliably induce an upward shift in the central corneal shape and wavefront modulation. This would extend the depth-of-focus without compromising the optical quality of the eye for distance vision.

2 | Experimental Session

Eleven human eye globes, not suitable for transplantation, were obtained from the Veneto Eye Bank Foundation (Venezia Zelarino, Italy). The eye globes were explanted between 6 and 12 h after death and immediately preserved at 4°C in corneal storage medium enriched with 15% dextran. All tissues were used for experiments within 48 h. All human eyes were used in compliance with the guidelines of the Declaration of Helsinki for research involving the use of human tissue.

2.1 | Theranostic-Guided UV-A Light Corneal Photo-Reshaping Procedure

Six eye globes with intact epithelium underwent theranostic-guided UV-A light corneal photo-reshaping procedure using a theranostic UV-A device (product code RS00VEI05, Regensight srl). The theranostic platform is equipped with an accessory corneal iontophoresis device (DoRSight, Regensight srl) for patterned delivery of a 0.22% riboflavin ophthalmic formulation (RitSight, Regensight srl) into the corneal stroma through the intact epithelium. The device integrates a sophisticated system enabling the simultaneous UV-A light-mediated measurement of riboflavin concentration distribution and the photo-activation of the substance within the corneal stroma. The theranostic UV-A device enables precise targeting of specific areas, such as the prepupillary area of the cornea, using an integrated blue light Placido disk system and an amber-led illumination system. This ensures that the treatment is accurately directed toward the desired corneal region to reshape. The key operational steps of the theranostic procedure are summarized in the following paragraph and depicted in Figure 1. The first step consisted of focusing the Placido rings of the integrated corneal topography system of the device onto the cornea through the interaction with an augmented reality system displayed on the touchscreen. Once focusing was completed, an image of the central 5.0 mm of the cornea to treat was acquired by pressing the footswitch to activate a 3 mW/cm^2 UV-A light irradiance for 2 s; the measure was recorded as baseline corneal fluorescence signal from the UV-A theranostic device [20, 21]. Therefore, the application of the corneal iontophoresis system was done under amber-led light illumination to center it onto the pupil of the eye. Application of the active electrode, which is embedded in the inner bath tube, followed to the suctioning of the outer segment to the limbus. The inner tube was placed onto the corneal surface, passing through the outer segment; it was then filled with the 0.22% riboflavin ophthalmic solution. The distal end of the inner tube was designed with apertures of various sizes and shapes to enhance the penetration of riboflavin into the pericentral targeted volume of the cornea rather than the central tissue volume. The application time and the sizes and shapes of distal apertures were determined

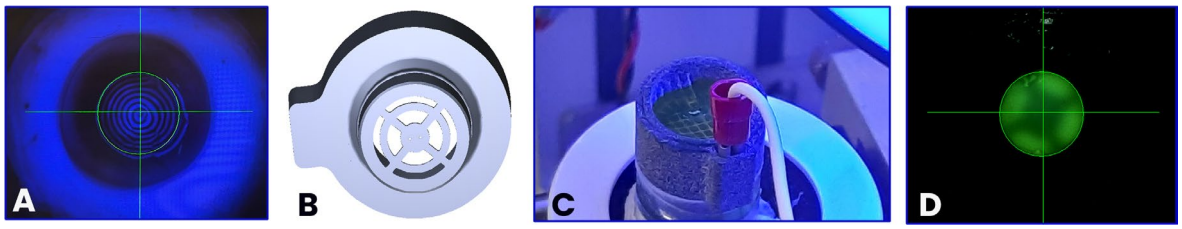

FIGURE 1 | Testing procedure: The donor human eye globe was mounted on a custom-designed eye holder and preconditioned. The eye holder could be tilted 90° to perform corneal topography. The corneal iontophoresis delivery system consists of (A) an outer segment, which is suctioned onto the eye after centering it on the pupil center using the integrated illumination system of the optical head and (B) an inner segment, which (C) is filled with 0.22% riboflavin ophthalmic formulation and connected via cable to the theranostic UV-A medical device. (D) At the end of application time, the inner segment is removed, the excess riboflavin is thoroughly dried with a Merocel sponge, and the riboflavin corneal concentration distribution is measured by theranostic UV-A device. The system allows, under a controlled low-current field generated by the theranostic UV-A device, for precise, spatial patterned delivery of riboflavin with lower levels in the central zone than surrounding zones of the treated cornea.

experimentally to reach a targeted spatial concentration distribution of riboflavin in the corneal stroma (data not published). The passive electrode of the iontophoresis device, consisting of a crocodile clip, was clamped to the optic nerve. Once placed onto the eye, the delivery device was controlled through the graphic user interface (GUI) of the theranostic UV-A device; the current intensity generated by the active device could be controlled between 0.5 and 2.0 mA depending upon the inner resistance of the eye. The duration of iontophoresis delivery was 7 min in all cases.

At the end of application time, the delivery device was removed from the eye globe and the UV-A theranostic platform provided the operator with a measure estimating the riboflavin spatial concentration distribution over 5.0 mm area by irradiating the cornea under treatment with 3 mW/cm^2 UV-A power density for 2 s. Therefore, the cornea underwent 10 mW/cm^2 UV-A irradiance for 9 min (5.4 J/cm^2 UV-A light energy dose) with a 5.0 mm diameter beam. At specified time intervals during irradiation, the theranostic UV-A device assessed the amount of riboflavin photo-activated. These measurements were performed over a 5.0 mm area of the cornea by exposing the treated region to UV-A light at a power density of 3 mW/cm^2 for 2 s.

2.2 | Controls

Standard CXL treatment, involving the manual application of riboflavin ophthalmic solution and UV-A light irradiation to de-epithelialized corneas was performed on four eye globes ($n = 4$), and data analyzed as a control for the study's hypothesis (positive control). Control eye globes were de-epithelialized using the Amoil's brush and, after baseline acquisition of corneal topography/aberrometry, underwent 30 min stromal soaking with 0.1% riboflavin ophthalmic solution (Ricrolin+, Sooft Italia Spa) and UV-A light irradiation at 3 mW/cm^2 UV-A irradiance for 30 min with an irradiation area of 9.0 mm diameter, which is the standard CXL protocol [24], using theranostic UV-A device.

To exclude any confounding factors related to the iontophoresis procedure itself and to further test the study's hypothesis, one donor human eye (negative control) underwent controlled corneal iontophoresis with sterile water for injection (application time: 7 min) and UV-A irradiation at 10 mW/cm^2 for 9 min (beam size: 5 mm).

UV-A light irradiation protocols used in the study and control eyes delivered the same total UV-A energy density of 5.4 J/cm^2 to the cornea. No riboflavin drop was instilled over the corneal surface during UV-A light irradiation in any sample.

2.3 | Testing Procedure

Each eye globe was kept in a 15% dextran-enriched storage solution at room temperature for 30 min before commencing the experiment. The eye globe was then gently mounted into a specially designed holder, with known vertical/horizontal orientation, to guarantee proper centration during the topography measurements. The intraocular pressure (IOP) of the eye globe was adjusted to 18 mmHg by means of a water column, which was connected via a needle to the optic nerve and filled with sterile water for injection. Before the experiment, the pressure of each eye globe was kept constant at 18 mmHg for 20 min to achieve a unique *prestressing* reference state of the corneal tissue before testing [25–27]. The same eye pressure of 18 mmHg was kept constant for the entire duration of the experiment. A commercial air conditioner heat pump was used to maintain the room temperature and humidity constant during the experiment.

Central corneal thickness (CCT) was acquired by anterior-segment OCT imaging (AS-OCT; HS-100, Canon) and corneal topography was performed using a Placido disk topographer (Keratron Scout, Optikon 2000). AS-OCT and corneal topography maps were taken at baseline (after the *prestressing* procedure) and 2 h after treatment. The elevation maps were evaluated by using the internal software of the topographer. Elevation data were expressed using the best-fit sphere (BFS) in diopters (D); the BFS corresponds to the virtual spherocylindric surface that best-fits the axial map over central 3.0 mm [28]. In Keratron topographer, the BFS corresponds to the average of the simulated keratometry values, $SimK_{steep}$ and $SimK_{flat}$ values, which are the average dioptric values of the 3 mm central rings of the major and minor axes, respectively. The system calculates the relative elevation based on the deviation of the axial map from the BFS; subtraction elevation maps using BFS have been found to be accurate for capturing subtle variations in surface geometry, making them valuable when the true topography must be known [29]. In this study, height difference maps were generated by comparing elevation data recorded at baseline and 2 h after

TABLE 1 | Main laboratory findings.

Sample code	Central riboflavin concentration (μg/cm³)	±2.5 mm zone riboflavin concentration (μg/cm³)	Corneal BFS at baseline (D)	Corneal BFS after treatment (D)	Shift (upward: +; downward: −) at vertex point of corneal height difference maps (μm)
Study eye Code 222412	80	186	43.99	44.81	+21.3
Study eye Code 222414	80	192	41.06	41.67	+16.2
Study eye Code 222482	68	132	42.54	43.70	+9.0
Study eye Code 223518	82	296	43.53	44.15	+12.7
Study eye Code 230994	93	208	40.64	41.30	+8.6
Study eye Code 171022	72	188	43.95	44.80	+14.0
$M \pm SD$	80 ± 9	200 ± 53	42.6 ± 1.5	43.4 ± 1.5[†]	13.6 ± 4.8
Control eye Code 182958	203	188	42.58	42.44	−10.1
Control eye Code 183048	208	203	44.44	44.49	+1.5
Control eye Code 183773	143	138	42.58	42.44	−10.3
Control eye Code 184531	140	140	44.49	44.44	−1.0
$M \pm SD$	173 ± 37	167 ± 33	43.5 ± 1.1	43.5 ± 1.2	−5.0 ± 6.1

Note: For both the study and positive control (standard CXL) groups, data are summarized as mean (M) ± standard deviation (SD).
Abbreviation: BFS: best-fit sphere.
[†]$p < 0.001$.

treatment. To eliminate tilt, the maps were aligned at three reference points at 7 mm (i.e., outside the treatment zone) from the vertex point ($x=0; y=0$), which corresponds to the highest point in corneal elevation. The difference value at the vertex points of the keratograph, expressed in micrometers (μm), was used for analysis. The topographer software calculates the corneal wavefront aberration (WA) on the corneal elevation with respect to an ideal aspherical corneal shape with eccentricity $1/n$ (where $n=1.3375$) and centered on the corneal vertex. The corneal WA was computed with respect to the center of the entrance pupil and obtained using a least-squares best-fit procedure to a 5.0 mm pupil area and described as a seventh-order Zernike polynomial expansion, excluding first- and second-order terms [30–32]. The root mean square (RMS) errors of corneal primary and secondary spherical aberration, coma, trefoil, and total high-order aberration values at 5.0 mm pupil diameter were used for statistical analysis. The radial modulation transfer function (MTF) was computed from the corneal high-order WA (at $\lambda=555$ nm) both before and after treatment. The Stiles-Crawford effect was incorporated into the calculation, using $r=0.05\,\text{mm}^{-2}$ as the shape factor value [30]. The MTF was reduced to a one-dimensional graph, a process called *radial averaging* (*r*MTF), as described in previous reports [30, 33]. This process allows us to quantify and reveal the optical quality of the cornea by looking at how fast the *r*MTF degrades as spatial frequency increases. In addition, the MTF ratio, which was calculated by dividing the preoperative radial MTF data by the postoperative MTF data, served as an optical performance index to quantify the treatment effect on the optical quality of the cornea across spatial frequencies ranging from 0 to 60 cycles per degree (cpd) [30, 33]. A value higher than 1 means that a decline in the optical quality has occurred in corneal optics, whereas a value less than 1 indicates an improvement in optical quality.

2.4 | Statistics

Data were expressed as mean ± standard deviation with 95% confidence intervals. The sample size was calculated to obtain a mean difference of 10 μm (SD 30%) between the vertex point in subtraction elevation topography maps (i.e., treatment map minus baseline map). A minimum sample size of five eye globes was needed to achieve 95% statistical power (β) at a statistical significance of 5% (α). The targeted mean difference of 10 μm in height difference maps after the 5.0 mm size treatment zone was determined according to the notion that it corresponds to a 1.0 D change in corneal power on the optical axis [34]. Baseline and postoperative BFS and high-order aberration data were compared using paired *t*-tests. The coefficient of variation (CoV) was calculated to estimate the reliability of the procedure.

3 | Results and Discussion

Human donor eye bank tissues were used in a controlled environment, and treatment response of the anterior cornea was measured using Placido disk technology after accurately orienting the cornea and under monitored IOP [23, 35]. All samples

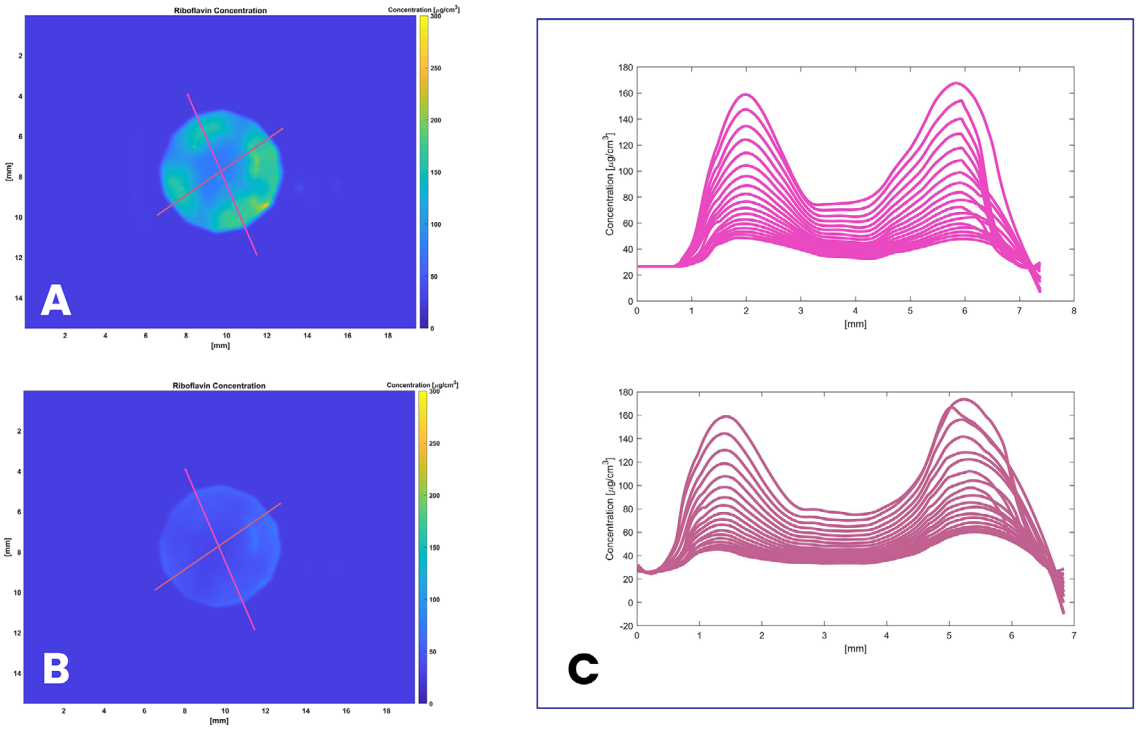

FIGURE 2 | Delivery of riboflavin into the cornea through the corneal iontophoresis-controlled system allows for achieving targeted concentration distribution of the substance into the cornea with an average of 60% lower levels in the central zone of the treated cornea compared to the surrounding area (±2.5 mm from center). Panels (A) and (B) illustrate the real-time theranostic UV-A device monitoring system and the corneal riboflavin concentration distribution at the beginning and at the end of application time, respectively (the bars indicate concentration in $\mu g/cm^3$). In (C), the corneal riboflavin concentration profiles are measured during theranostic-guided UV-A light irradiation along two axes (purple and red lines in A and B, respectively). Each curve represents a measure (taken every 30 s).

underwent thorough testing and the process was successfully completed in all cases. The mean donor age was 64 ± 14 years. The mean cadaver time was 9 ± 5 h. At baseline, the mean CCT was 583 ± 58 μm; it did not change at the end of experiments (596 ± 69 μm). The outcome data of the laboratory study are summarized in Table 1.

The study hypothesized that the spatial concentration gradient of riboflavin within the corneal stroma could drive the photopolymerization process under theranostic UV-A light-mediated illumination of the cornea, leading to a predictable change in corneal shape and WA. For this purpose, riboflavin was applied in a patterned, spatially precise manner using a controlled corneal iontophoresis delivery system connected to the theranostic device. At the end of corneal iontophoresis delivery, the average corneal riboflavin concentration was 80 ± 9 μg/cm^3 in the central area and 200 ± 53 μg/cm^3 at ±2.50 mm from the center, resulting in a consistent concentration ratio of 0.4 ± 0.1 (Figure 2). Consequently, theranostic-guided UV-A light irradiation photo-activated an average of 28% ± 12% (57 ± 12 μg/cm^3) of riboflavin in the central corneal region and 45% ± 17% (115 ± 49 μg/cm^3) in the surrounding region, ±2.50 mm from the center. This variation in riboflavin concentration photo-activation led to differing amounts and spatial distributions of cross-linking bonds among stromal proteins, resulting in varying levels of corneal strengthening across adjacent tissue areas [36, 37]. In this study, the UV-A light irradiation protocol was the same for all eyes, ensuring that the primary hypothesis of the study was accurately tested and any observed effects could be attributed directly to the gradient concentration distribution of stromal riboflavin. The central cornea significantly steepened by 0.8 D ($p < 0.001$), from 42.6 ± 1.5 D to 43.4 ± 1.5 D, immediately after treatment, with a consistent upward height shift of +13.6 ± 4.8 μm (95% CI: 11.3–15.2 μm; CoV: 3.7%; Figure 3). A significant average 50% decrease of primary spherical aberration, from 0.14 ± 0.07 μm to 0.07 ± 0.06 μm (−0.07 ± 0.04 μm; $p = 0.005$), was measured over 5.0 mm pupil area. No significant changes were measured in RMS errors of corneal secondary spherical aberration ($p = 0.64$), coma ($p = 0.82$), trefoil ($p = 0.47$), and total high-order aberration ($p = 0.83$), as summarized in Table 2. The theranostic procedure induced smooth corneal wavefront shaping, with the WA distinctly advanced near the periphery of the 5.0 mm pupil compared to the central area (Figure 4). After treatment, the radial MTF remained almost unchanged at all frequencies with respect to preoperatively, indicating that the procedure did not compromise the image optical quality of the anterior cornea (Figure S1). This finding was further evidenced by the MTF ratio analysis (Figure 5).

In controls treated by standard CXL procedure, the eye globes achieved a uniform corneal riboflavin concentration with values of 174 ± 37 μg/cm^3 and 167 ± 33 μg/cm^3 at the center and ±2.50 mm surrounding zone, respectively. The BFS (−0.1 ± 0.1 D; $p = 0.21$) and the corneal apex point (−5.0 ± 6.1 μm) did not significantly change with respect to the baseline (Figure S2). No changes in RMS errors of corneal primary spherical aberration ($p = 0.90$), corneal secondary spherical aberration ($p = 0.11$), coma ($p = 0.48$), trefoil ($p = 0.49$), and total high-order aberration ($p = 0.59$) were found in the control group (Table 2). The radial MTF slightly

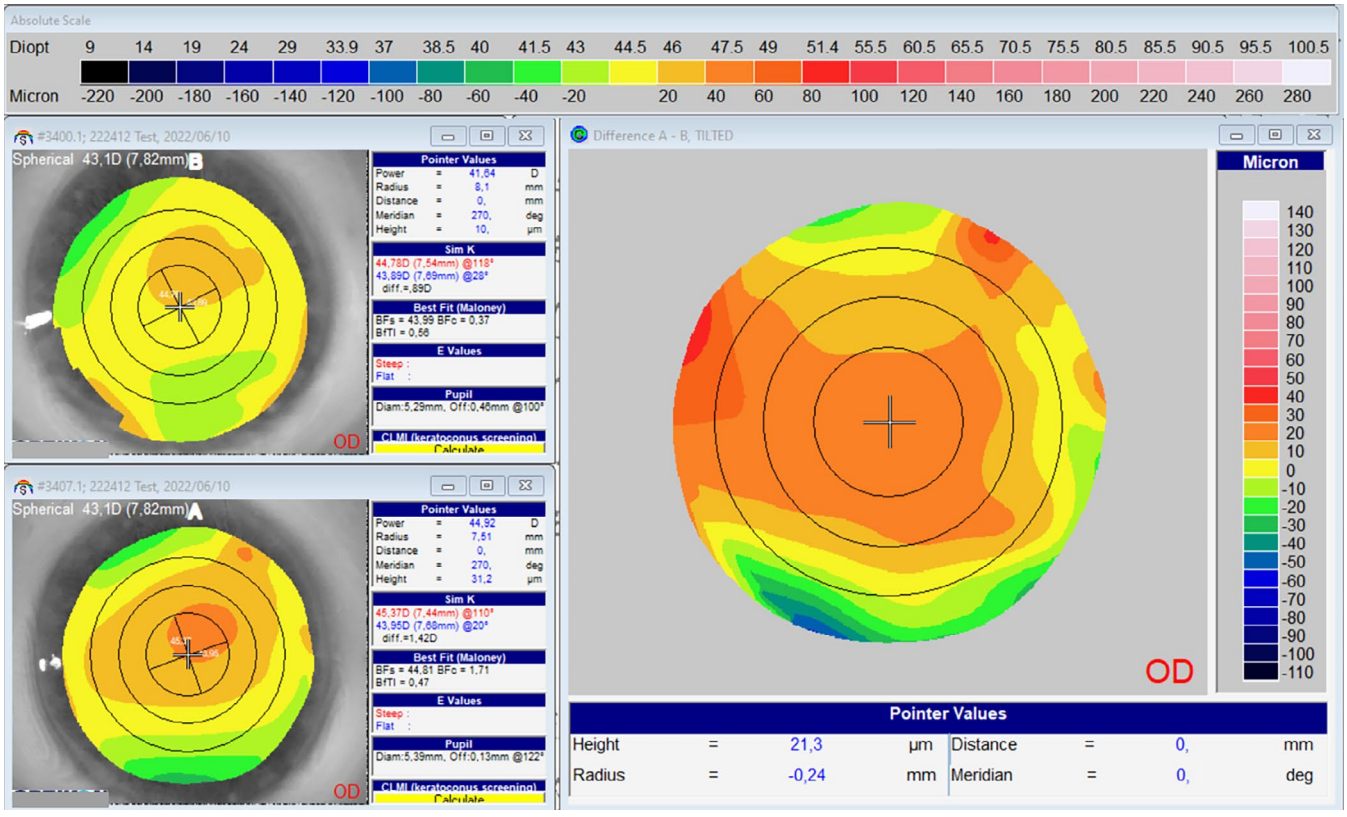

FIGURE 3 | The differential elevation topography map for sample code 222412 (refers to Table 1) demonstrated a significant central upward shift of 21.3 μm following theranostic-guided UV-A light corneal photo-reshaping. This result was achieved through spatially targeted delivery of 0.22% riboflavin and a 5.0 mm UV-A light beam irradiation. This finding demonstrated a measurable change in the anterior corneal topography of the study sample after treatment. The panels (A) and (B) illustrate the postoperative and preoperative corneal elevation maps, respectively.

TABLE 2 | Changes in root mean square (RMS) errors of corneal wavefront high-order aberrations.

Group	HOA	Primary SA	Secondary SA	Coma	Trefoil
Study group	−0.01 ± 0.12 μm	−0.07 ± 0.04 μm*	−0.01 ± 0.03 μm	+0.02 ± 0.14 μm	+0.02 ± 0.06 μm
Control group (standard CXL)	+0.03 ± 0.09 μm	+0.01 ± 0.04 μm	+0.03 ± 0.02 μm	−0.04 ± 0.10 μm	+0.03 ± 0.08 μm

Note: For both study and positive control groups, data are summarized as mean (M) ± standard deviation (SD).
Abbreviations: HOA: total cornea high-order aberrations; SA: spherical aberration.
*$p < 0.05$.

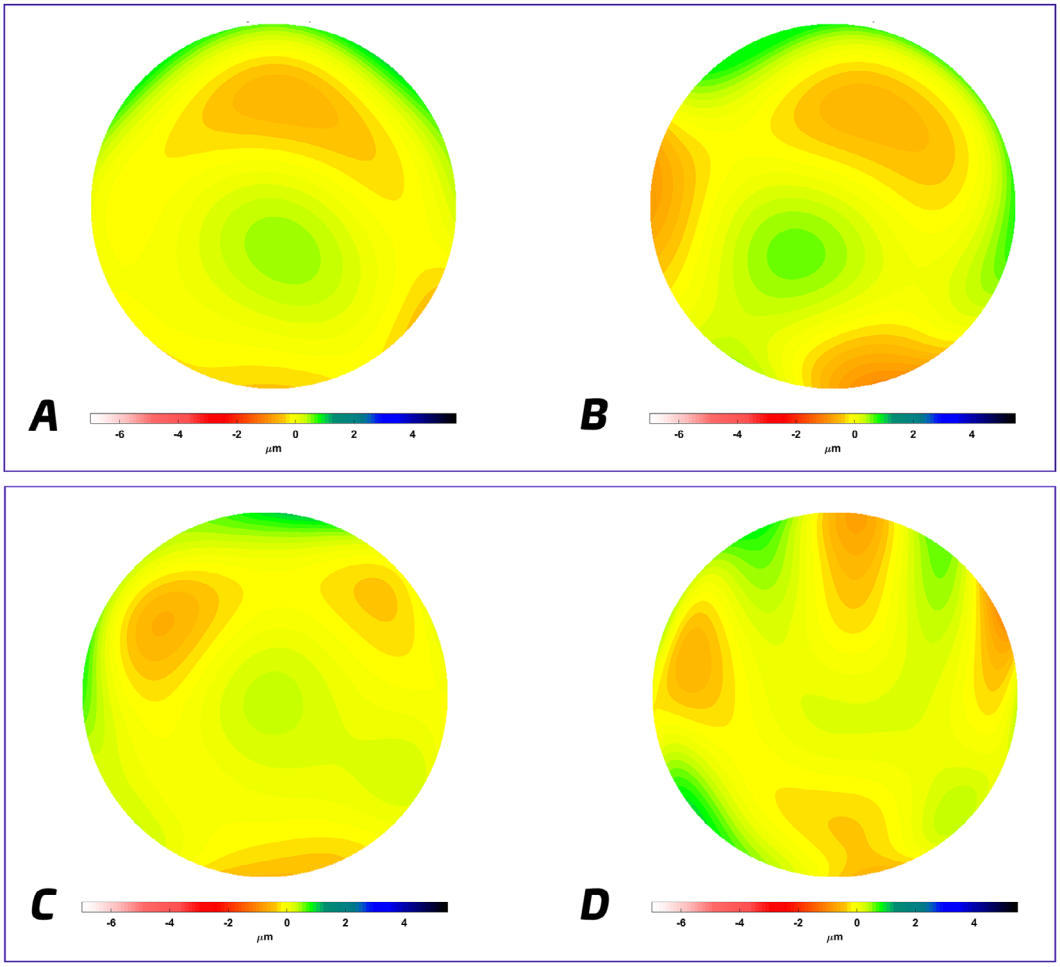

FIGURE 4 | Average corneal high-order WA maps of study and control groups, before (A and C) and after (B and D) testing procedures over 5.0 mm pupil size. After theranostic-guided UV-A light corneal photo-reshaping combined with controlled delivery of riboflavin, (B) the corneal high-order WA distinctly advanced near the periphery of the 5.0 mm pupil compared to the central area, while spherical aberration decreased. In the positive control group, the corneal high-order WA changed after the standard CXL procedure, (D) but no consistent pattern was observed. A fixed color scale, visually similar to that of commercial corneal aberrometers, was developed for easy interpretation (scale bars in microns, range between −7 and +5 μm).

decreased at intermediate and higher frequencies after standard CXL treatment, as confirmed by the MTF ratio analysis. In the negative control eye (code 184518), which received sterile water and UV-A irradiation under the same treatment settings as the study eyes, no change was observed in BFS (0.05 D) or corneal height (0.0 μm). This result confirmed the role of patterned riboflavin concentration combined with UV-A irradiation in precisely and accurately modulating corneal shape and WAs (Figure S3).

It has been shown that the concentration of riboflavin plays a crucial role in generating covalent chemical bonds between stromal proteins in the cornea [17–19, 23]. Authors have predicted that under appropriate photo-activation by UV-A light, the tissue biomechanical response could be selectively differentiated according to the controlled spatial distribution of riboflavin concentration and may cause the cornea to deform to a defined shape [38–40]. By precisely controlling the UV-A light and the pattern of riboflavin delivery, specific areas of the cornea could be targeted to achieve the desired optical correction. In the previous study [23], we demonstrated a predictable and reproducible corneal shape change for correction of myopic defocus in donor eye bank human eyes using a delivery system with the central pore wider

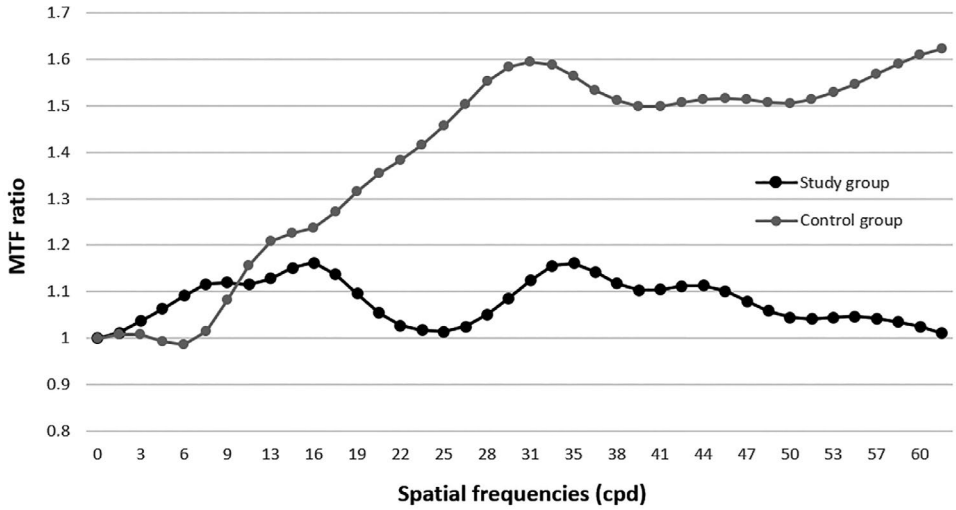

FIGURE 5 | MTF ratio curves over 5.0 mm pupil size. Data are represented both for the study (black dots) and the positive control group (gray dots) at spatial frequencies ranging from 0 to 60 cpd. Theranostic-guided UV-A light corneal photo-reshaping did not degrade optical quality (MTF ratio ≈ 1) showing a sinusoidal shape along mid- and high-spatial frequencies. After standard CXL, the MTF ratio showed high values gradually increasing from mid-spatial (≥ 10 cpd) to high-spatial (≥ 30 cpd) frequencies.

than pericentral pores. In this study, we confirmed the ability to pattern the delivery of riboflavin into the human cornea using a new, purpose-designed delivery system, with pericentral pores wider than the central pore. This delivery device was tested for its effectiveness in theranostic-guided UV-A light corneal photo-reshaping, with the goal of potentially compensating for the loss of lens accommodation associated with presbyopia and improving the near vision ability of the human eye. To confirm this hypothesis, control eyes, which underwent either standard CXL treatment or sham treatment using the same UV-A light energy dose, did not show any immediate change in corneal shape or WA. Future research could investigate variations in UV-A light energy and fluence rates to gain a deeper understanding of their potential impact on treatment outcomes.

The central 2.0 mm corneal WA was delayed following the theranostic procedure, likely due to the changes in curvature that increased the optical path length. In contrast, the surrounding 5.0 mm corneal zone of WA advanced, reducing the optical path length. This, combined with a significant reduction in positive spherical aberration over 5.0 mm pupil (i.e., mesopic pupil size), contributed to an extended focal range across the cornea. Despite this wavefront shaping, MTF analysis indicated that the overall optical performance of the cornea remained stable at intermediate and high frequencies. This stability implies that image resolution and sharpness across distances, from distance to intermediate, and potentially near vision, can be achieved following this novel approach. A similar principle of operation has been exploited in the design of an extended-depth-of-focus (EDoF) IOL [41]. Interestingly, two randomized controlled clinical trials (NCT03010254 and NCT03274986) indicated superior mean monocular distance-corrected visual acuity at intermediate distance (DCIVA) and non-inferior corrected distance visual acuity (CDVA) in subjects after bilateral implantation of wavefront-shaping EDOF versus monofocal IOL ($n = 282$ and $n = 218$, respectively) [42, 43]. The advantage of an incision-free corneal approach over an IOL implant is that it directly addresses the primary source of high-order optical aberrations in the eye, that is, the anterior cornea, through an incision-free procedure. Furthermore, the theranostic corneal approach could enhance the overall optical quality by reducing positive spherical aberration, which may improve the effectiveness of subsequent IOL implantation if needed, without affecting the choice of the IOL [44]. This novel approach could be further investigated as a method to improve optical quality in eyes with significant optical aberrations, particularly those with high positive spherical aberration, following corneal radial keratotomy for keratoconus or laser vision correction for high myopia.

4 | Conclusion

In conclusion, we demonstrated the feasibility of an incision-free, corneal approach, based on theranostic technology, for presbyopia correction. This method enhances the optical properties of the cornea without altering its thickness, providing an in-office procedure that avoids tissue removal or incisions. In addition, it does not require expensive laser equipment and can be repeated as needed to address the progressive nature of presbyopia. This technique would provide a practical and safe solution for the long-term management of this age-related condition. A clinical study is necessary to investigate the effectiveness of this novel technology in compensating for the loss of lens accommodation and improving near vision in presbyopic individuals.

Author Contributions

Giuseppe Lombardo and Marco Lombardo were involved in conceptualization, investigation, writing original draft, and project management. Sebastiano Serrao and Giuseppe Massimo Bernava were involved in investigation, data analysis, review, and editing original draft.

Acknowledgments

Open access publishing facilitated by Consiglio Nazionale delle Ricerche, as part of the Wiley - CRUI-CARE agreement.

Conflicts of Interest

Marco Lombardo and Giuseppe Lombardo are coinventors on issued patents (IT102019000011985, CN114126650, and US20230131004) related to this work. Sebastiano Serrao and Giuseppe Massimo Bernava declare no conflicts of interest.

Data Availability Statement

The research data associated with this study are not publicly available.

References

1. M. Markoulli, T. R. Fricke, A. Arvind, et al., "BCLA CLEAR Presbyopia: Epidemiology and Impact," *Contact Lens & Anterior Eye* 47 (2024): 102157.

2. K. D. Frick, S. M. Joy, D. A. Wilson, K. S. Naidoo, and B. A. Holden, "The Global Burden of Potential Productivity Loss From Uncorrected Presbyopia," *Ophthalmology* 122, no. 8 (2015): 1706–1710.

3. K. Sioufi, L. Zheleznyak, S. MacRae, and K. M. Rocha, "Femtosecond Lasers in Cornea & Refractive Surgery," *Experimental Eye Research* 205 (2021): 108477.

4. L. R. Stival, M. N. Figueiredo, and M. R. Santhiago, "Presbyopic Excimer Laser Ablation: A Review," *Journal of Refractive Surgery* 34, no. 10 (2018): 698–710.

5. R. Shetty, S. Brar, M. Sharma, Z. Dadachanji, and V. G. Lalgudi, "PresbyLASIK: A Review of PresbyMAX, Supracor and Laser Blended Vision: Principles, Planning, and Outcomes," *Indian Journal of Ophthalmology* 68, no. 12 (2020): 2723–2731.

6. V. Vargas-Fragoso and J. L. Alio, "Corneal Compensation of Presbyopia: PresbyLASIK: An Updated Review," *Eye and Vision* 4 (2017): 11.

7. M. Moshirfar, M. K. Henrie, C. J. Payne, et al., "Review of Presbyopia Treatment With Corneal Inlays and New Developments," *Clinical Ophthalmology* 16 (2022): 2781–2795.

8. F. F. N. Keskin Perk, S. Taneri, C. Tanriverdi, S. Haciagaoglu, Z. Y. Karaca, and A. Kilic, "Increasing Depth of Focus With Allogeneic Presbyopic Inlays: 3-Year Results," *Journal of Cataract and Refractive Surgery* 49, no. 10 (2023): 1005–1010.

9. A. P. Papadopoulos and A. P. Papadopoulos, "Current Management of Presbyopia," *Middle East African Journal of Ophthalmology* 21, no. 1 (2014): 10–17.

10. M. C. Sánchez-González, E. Gutiérrez-Sánchez, J. M. Sánchez-González, et al., "Complications of Small Aperture Intracorneal Inlays: A Literature Review," *Life (Basel)* 13, no. 2 (2023): 312.

11. B. J. Fenner, A. S. Moriyama, and J. S. Mehta, "Inlays and the Cornea," *Experimental Eye Research* 205 (2021): 108474.

12. F. D'Oria, J. L. Alio, A. Martinez-Abad, L. Izquierdo, Jr., P. Larco, Jr., and A. A. Abdelghany, "Astigmatic Change as a Predictor of Intrastromal Corneal Ring Segment Late Extrusion," *Journal of Cataract and Refractive Surgery* 48, no. 4 (2022): 401–407.

13. T. T. Du, V. C. Fan, and P. A. Asbell, "Conductive Keratoplasty," *Current Opinion in Ophthalmology* 18, no. 4 (2007): 334–337.

14. D. Zamora-de La Cruz, J. Bartlett, M. Gutierrez, and S. M. Ng, "Trifocal Intraocular Lenses Versus Bifocal Intraocular Lenses After Cataract Extraction Among Participants With Presbyopia," *Cochrane Database of Systematic Reviews* 1, no. 1 (2023): CD012648.

15. B. Orman and G. Benozzi, "Pharmacological Treatments for Presbyopia," *Drugs & Aging* 40, no. 2 (2023): 105–116.

16. J. I. Barraquer, "Modification of Refraction by Means of Intracorneal Inclusions," *International Ophthalmology Clinics* 6, no. 1 (1966): 53–78.

17. P. Kamaev, M. D. Friedman, E. Sherr, and D. Muller, "Photochemical Kinetics of Corneal Cross-Linking With Riboflavin," *Investigative Ophthalmology & Visual Science* 53 (2012): 2360–2367.

18. J.-T. Lin, "A Critical Review on the Kinetics, Efficacy, Safety, Nonlinear Law and Optimal Protocols of Corneal Crosslinking," *Journal of Ophthalmology & Visual Neuroscience* 3 (2018): 1–10.

19. J. T. Lin, "A Proposed Concentration-Controlled New Protocol for Optimal Corneal Crosslinking Efficacy in the Anterior Stroma," *Investigative Ophthalmology & Visual Science* 59 (2018): 431–432.

20. G. Lombardo, G. M. Bernava, S. Serrao, A. M. Roszkowska, and M. Lombardo, "Predicting Corneal Cross-Linking Treatment Efficacy With Real-Time Assessment of Corneal Riboflavin Concentration," *Journal of Cataract and Refractive Surgery* 49, no. 6 (2023): 635–641.

21. G. Lombardo, G. M. Bernava, S. Serrao, and M. Lombardo, "Theranostic-Guided Corneal Cross-Linking: Pre-Clinical Evidence on a New Treatment Paradigm for Keratoconus," *Journal of Biophotonics* 15, no. 12 (2022): e202200218.

22. A. M. Roszkwoska, V. Scorcia, R. Mencucci, et al., "Assessment of the Predictive Ability of Theranostics for Corneal Cross-Linking in Treating Keratoconus: A Randomized Clinical Trial," *Ophthalmology* 131, no. 12 (2024): 1403–1415.

23. M. Lombardo, S. Serrao, G. M. Bernava, and G. Lombardo, "Spatial Targeted Delivery of Riboflavin With a Controlled Corneal Iontophoresis Delivery System in Theranostic-Guided UV-A Light Photo-Therapy," *Journal of Biophotonics* 17, no. 7 (2024): e202400068.

24. M. Lombardo, G. Pucci, R. Barberi, and G. Lombardo, "Interaction of Ultraviolet Light With the Cornea: Clinical Implications for Corneal Crosslinking," *Journal of Cataract and Refractive Surgery* 41, no. 2 (2015): 446–459.

25. B. L. Boyce, R. E. Jones, T. D. Nguyen, and J. M. Grazier, "Stress-Controlled Viscoelastic Tensile Response of Bovine Cornea," *Journal of Biomechanics* 40 (2007): 2367–2376.

26. B. L. Boyce, J. M. Grazier, R. E. Jones, and T. D. Nguyen, "Full-Field Deformation of Bovine Cornea Under Constrained Inflation Conditions," *Biomaterials* 29 (2008): 3896–3904.

27. H. Hennighausen, S. T. Feldma, J. F. Bille, and A. D. McCulloch, "Anterior-Posterior Strain Variation in Normally Hydrated and Swollen Rabbit Cornea," *Investigative Ophthalmology & Visual Science* 39 (1998): 253–262.

28. R. K. Maloney, S. J. Bogan, and G. O. Waring, "Determination of Corneal Image-Forming Properties From Corneal Topography," *American Journal of Ophthalmology* 115 (1993): 31–41.

29. T. O. Salmon and D. G. Horner, "Comparison of Elevation, Curvature, and Power Descriptors of Corneal Topographic Mapping," *Optometry and Vision Science* 72, no. 11 (1995): 800–808.

30. M. Lombardo and G. Lombardo, "The Wave Aberration of Human Eyes and New Descriptors of Image Optical Quality and Visual Performance," *Journal of Cataract and Refractive Surgery* 36 (2010): 313–331.

31. L. N. Thibos, X. Hong, A. Bradley, and R. A. Applegate, "Accuracy and Precision of Objective Refraction From Wavefront Aberrations," *Journal of Vision* 4, no. 4 (2004): 329–351.

32. F. Yi, D. R. Iskander, and M. Collins, "Depth of Focus and Visual Acuity With Primary and Secondary Spherical Aberration," *Vision Research* 51 (2011): 1648–1658.

33. M. Lombardo, G. Lombardo, and S. Serrao, "Long-Term Optical Quality of the Photoablated Cornea," *Journal of the Optical Society of America. A, Optics, Image Science, and Vision* 24 (2007): 588–596.

34. C. R. Munnerlyn, S. J. Koons, and J. Marshall, "Photorefractive Keratectomy: A Technique for Laser Refractive Surgery," *Journal of Cataract and Refractive Surgery* 14, no. 1 (1998): 46–52.

35. A. Alarcon, C. Canovas, R. Rosen, et al., "Preclinical Metrics to Predict Through-Focus Visual Acuity for Pseudophakic Patients," *Biomedical Optics Express* 7 (2016): 1877–1888.

36. J. Ø. Hjortdal and N. Ehlers, "Effect of Excimer Laser Keratectomy on the Mechanical Performance of the Human Cornea," *Acta Ophthalmologica Scandinavica* 73 (1995): 18–24.

37. M. K. Smolek, "Interlamellar Cohesive Strength in the Vertical Meridian of Human Eye Bank Corneas," *Investigative Ophthalmology & Visual Science* 34 (1993): 2962–2969.

38. J.-T. Lin and D.-C. Cheng, "Modeling the Efficacy Profiles of UV-Light Activated Corneal Collagen Crosslinking," *PLoS One* 12, no. 4 (2017): e0175002.

39. R. Schumacher, M. Mrochen, J. Wernli, M. Bueeler, and T. Seiler, "Optimization Model for UV-Riboflavin Corneal Cross-Linking," *Investigative Ophthalmology & Visual Science* 53 (2012): 762–769.

40. A. Semchisten, M. Mrochen, and V. Semchisten, "Model for Optimization of the UV-A/Riboflavin Strengthening (Cross-Linking) of the Cornea: Percolation Threshold," *Photochemistry and Photobiology* 91 (2015): 1403–1411.

41. T. Kohnen, J. P. Berdahl, X. Hong, and C. Bala, "The Novel Optical Design and Clinical Classification of a Wavefront-Shaping Presbyopia-Correcting Intraocular Lens," *Clinical Ophthalmology* 17 (2023): 2449–2457.

42. C. Bala, F. Poyales, M. Guarro, et al., "Multicountry Clinical Outcomes of a New Nondiffractive Presbyopia-Correcting IOL," *Journal of Cataract and Refractive Surgery* 48, no. 2 (2022): 136–143.

43. C. McCabe, J. Berdahl, H. Reiser, et al., "Clinical Outcomes in a U.S. Registration Study of a New EDOF Intraocular Lens With a Nondiffractive Design," *Journal of Cataract and Refractive Surgery* 11 (2022): 1297–1304.

44. L. Salvá, S. García, S. García-Delpech, A. Martínez-Espert, and V. Ferrando, "Optical Performance of a Segmented Extended-Depth-of-Focus Intraocular Lens Under the Influence of Different Values of Spherical Aberration Generated by Refractive Surgery," *Journal of Clinical Medicine* 12, no. 14 (2023): 4758.

Supporting Information

Additional supporting information can be found online in the Supporting Information section.